

Nearly perfect large-area quartz: 4 meV resolution for 10 keV photons over 10 cm²

John P. Sutter,^{a*} Alfred Q. R. Baron,^a Daigo Miwa,^b Yoshinori Nishino,^b
Kenji Tamasaku^b and Tetsuya Ishikawa^b

^aSpring-8/JASRI, 1-1-1 Kouto, Sayo-cho, Sayo-gun, Hyogo 679-5198, Japan, and ^bSpring-8/RIKEN, 1-1-1 Kouto, Sayo-cho, Sayo-gun, Hyogo 679-5148, Japan. E-mail: sutter@spring8.or.jp

The perfection of two commercial top-grade quartz crystal wafers has been investigated using Bragg reflection at $\theta_B = 89.77^\circ$ of a 2.0 meV bandwidth beam of 9.979 keV X-rays by the $(\bar{7}\bar{4}\bar{3}4)$ lattice planes. Topographic images show small defect concentrations ($\leq 5 \text{ cm}^{-2}$). Energy scan widths are below 3 meV over 8 mm \times 8 mm areas and 4 meV over the whole wafer ($\sim 11 \text{ cm}^2$). This suggests that quartz can be a useful optical material.

© 2006 International Union of Crystallography
Printed in Great Britain – all rights reserved

Keywords: quartz; backscattering; large area; low energy; high resolution.

1. Introduction

Silicon is often used for X-ray optical elements because large perfect-crystal ingots are readily available. However, its highly symmetric cubic lattice limits it in certain ways. Quartz, with its non-centrosymmetric trigonal lattice, offers an alternative. It can have notable advantages for high-energy resolution measurements (Sutter *et al.*, 2005) if perfect large-area crystals are available. Specific techniques that would benefit from quartz optics include high-resolution non-resonant inelastic X-ray scattering (IXS), resonant electronic IXS, and nuclear resonant scattering.

Most high-energy resolution measurements use crystals operating at Bragg reflections as close as possible to backscattering because this maximizes their angular acceptance (see, for example, Burkel, 1991). The low symmetry of the quartz lattice gives it many narrow-band-pass reflections at low photon energies. A single symmetric backscattering reflection of quartz could in principle provide 1 meV bandwidth at X-ray energies of less than 12 keV, while the smallest bandwidth available from silicon in this energy range is 9 meV. Thus quartz analyzers would make very high-resolution spectroscopy (*e.g.* phonon measurements) possible at smaller X-ray sources like Diamond, Soleil or NSLS-II, where the peak spectral flux is at lower energies. The lower symmetry of quartz also means that the atomic planes of quartz have a larger number of different spacings, yielding 184 distinct backscattering energies compared with 22 for silicon for 5–12 keV X-rays. For IXS techniques that tune the photon energy to an absorption edge, and for nuclear resonant scattering (Gerdau & de Waard, 1999), a backscattering reflection with the desired energy could be more easily found. Finally, the larger thermal expansion of quartz (three to five times larger than that of silicon, depending on crystal orientation) allows a larger energy scan range when temperature scans are used.

Backscattering from quartz has been investigated by Imai *et al.* (2001, 2002), and topography images have been made of synthetic quartz crystals (Yoshimura & Kohra, 1976; Yoshimura *et al.*, 1979). However, the former used a small beam and so does not show the degree of perfection over large areas, while the latter does not account for any advances made in the manufacture of quartz crystals

over the last quarter-century. Therefore, neither addresses the crucial unresolved issue of the availability of perfect quartz crystals of sufficient size, which would determine whether the notable advantages that quartz would in principle have over silicon could be realised. That is the question addressed here. We note that sapphire has also been considered and that in principle it shares some of the advantages of quartz (Shvyd'ko & Gerdau, 1999), but large-area perfect crystals such as those shown here do not seem to be readily available. Also, sapphire has generally wider bandpasses because of its larger Debye–Waller factors, resulting from its smaller mean square atomic displacements of $2.5 \times 10^{-3} \text{ \AA}^2$ for Al and $3.5 \times 10^{-3} \text{ \AA}^2$ for O (Lucht *et al.*, 2003). Because the mean square atomic displacements in quartz, though quite anisotropic (Kihara, 1990), are some three times greater ($7 \times 10^{-3} \text{ \AA}^2$ and $1.2 \times 10^{-2} \text{ \AA}^2$ for the Si and O atoms, respectively), the Debye–Waller factors of quartz, and with them the backscattering bandpasses, decline more quickly with increasing photon energy, making sapphire more interesting at higher energies.

This report contains both topographic images and reflectivity scans of the $(\bar{7}\bar{4}\bar{3}4)$ reflection of 9.979 keV photons in backscattering. The two wafers are 40 mm in diameter and 2.0 mm thick, and are polished on both sides. They are commercially available 'A-grade' crystals specified by the manufacturer (Tokyo Denpa) to have an oscillator Q -value of at least 2.5×10^6 (indicating low hydroxyl contamination), a density of 10–30 μm inclusions of at most 2 cm^{-3} , and a density of 30–70 μm inclusions of at most 1 cm^{-3} . Dynamical diffraction calculations yield a bandpass of 2.0 meV for this reflection if the quartz crystal is perfect and a monochromatic plane wave is assumed. The small structure factor that yields this narrow bandpass makes the extinction depth comparable with the absorption length of 210 μm ; the resulting strong absorption reduces the calculated peak reflectivity to 20%.

2. Apparatus

For this work the 1 km beamline BL29XUL of Spring-8 (Tamasaku *et al.*, 2001) was used. The X-ray source is a standard 4.5 m in-vacuum

undulator. A high-resolution monochromator was placed downstream from the high-heat-load monochromator, but still relatively close to the source. The beam from there was sent on to the hutch at 1 km from the source where the quartz wafers were placed. This provided a large-area, highly collimated and highly monochromatic X-ray beam.

The high-resolution monochromator, based on the design of Yabashi *et al.* (2001), was a four-crystal inline (+ n − n − n + n) Si monochromator using the (444) reflection ($\theta_B = 52.418^\circ$). The first pair of crystals was cut at an asymmetry angle of $+43.22^\circ$ ($b = -0.161$) to collimate the beam, while the second pair was cut with the opposite asymmetry. Calculations yielded full widths at half-maxima of 1.91 meV for the bandpass and $13.33 \mu\text{rad}$ for the angular acceptance. Each crystal was mounted on its own independent precision goniometer (0.01'' per step). The scattering plane was vertical. To vary the photon energy E , all four crystals were rotated. The factor $-E \cot \theta_B / 1000 = -7.679 \text{ meV } \mu\text{rad}^{-1}$ converted the angle of rotation into change in E .

The quartz wafer was mounted on a massive copper base and enclosed in a plastic cover with a Kapton window for protection against thermal fluctuations and air currents. This assembly was mounted on a double-axis goniometer to adjust its angle. The goniometer in turn was mounted on translation stages, allowing different parts of the wafer to be illuminated. The reflected beam could be recorded by either a CCD camera or an avalanche photodiode. Each of these two detectors was mounted on translation stages, allowing each one to be moved into the backscattered beam without moving the quartz wafer at all. The deviation of the quartz θ_B from exact backscattering was 0.23° for every topography image and energy scan.

3. Results and discussion

Fig. 1 shows a topograph covering most of the first quartz wafer. It is composed of individual topographs, each covering an $8 \text{ mm} \times 8 \text{ mm}$ area of the wafer. Each was taken by the CCD camera with a 10 s exposure.

Two features of this topograph should be noted. First, the lower left-hand corner of the wafer shows low reflection because the crystal lattice there differs from that elsewhere, as shown by the graph on the left-hand side of Fig. 1. Moreover, various defects can be seen. Most cover a small area, though a few, such as the vertical lines in the first row of images to the right of the center, extend over the whole diameter of the wafer. Each individual topograph is brightest at the lower right-hand corner because the incident beam is not quite uniform.

The reflectivity *versus* incident photon energy was measured with the $8 \text{ mm} \times 8 \text{ mm}$ incident beam at each region of the wafer imaged in the topograph in Fig. 1. It is clear that the peak widths had values between

2.9 and 4.0 meV. Summing these while properly accounting for temperature drifts yielded a peak of 4.0 meV FWHM. The sum of a Gaussian and a Lorentzian was chosen as the model curve for the summed peak because a perfect crystal would have an approximately Lorentzian energy curve, while the deviations from the perfect crystal could be expected to have a Gaussian distribution. We estimate that the intrinsic resolution of the quartz wafer is 3.5 meV by assuming that the four-bounce monochromator performs ideally.

A calculation of the quartz reflectivity from plane-wave dynamical theory, convoluted with the angle-integrated energy response of the high-resolution monochromator, is also contained in Fig. 1. The experimental energy curves have tails considerably stronger than the theory would predict. The range $\pm 5 \text{ meV}$ contains 89.44% of the integral of the summed curve from -40 meV to $+40 \text{ meV}$, while the corresponding figure for the calculated curve is 99.31%. It is unclear whether the tails arise from defects in the monochromator or the quartz wafer; further examination will be required.

To determine the effect of the small defects on the bandpass, two energy curves were taken from another quartz wafer with the incident beam slit down to $1 \text{ mm} \times 1 \text{ mm}$. One energy curve was taken at a part of the wafer with no visible defects. The other was taken at a typical defect (Fig. 2). Whereas the defect-free part of this

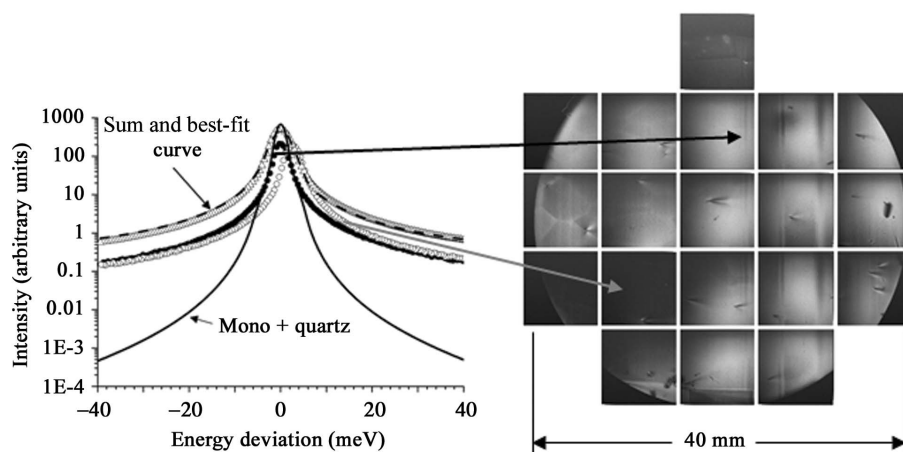


Figure 1

Topograph of quartz wafer with comparison of energy curves in two regions and sum of energy curves of all regions. The best-fit curve to the sum is a Gaussian of FWHM 4.17 meV centered at $+0.39 \text{ meV}$ plus a Lorentzian of FWHM 3.64 meV centered at -0.48 meV . The Gaussian peak amplitude is 0.994 times the Lorentzian peak amplitude. The convolution of the calculated quartz reflectivity with the angle-integrated high-resolution monochromator throughput has been included for reference.

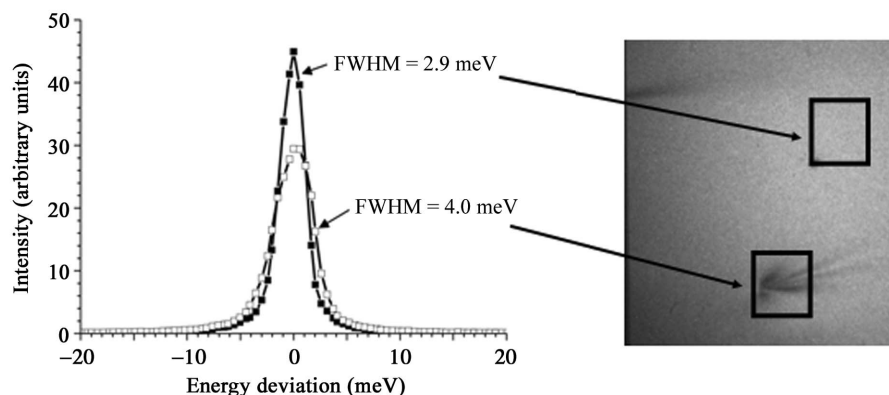


Figure 2

Comparison of defective and defect-free regions of a quartz wafer. See text.

wafer yields a reflectivity curve 2.9 meV wide, the defective part's 4.0 meV-wide reflectivity curve is both weaker and broader, indicating that the wafer's lattice structure is indeed strongly distorted at that spot.

Regarding these topographic images, some simple remarks can be made. At this Bragg angle of 89.77° the angular acceptance is large (50 μ rad). Therefore this type of topography will be mainly sensitive to variations in the interplanar spacing. In Fig. 1, the difference in the reflectivity peak positions of the top and lower left regions of the quartz wafer is 2.5 meV; this could be explained by a difference in lattice spacing of $2.5 \text{ meV}/9.979 \text{ keV} = 0.25 \text{ ppm}$. When the crystal was mounted more loosely later, this dark spot disappeared; mounting strain was probably therefore responsible for this feature. Furthermore, the extinction depth of 0.16 mm and the absorption length of 0.21 mm are comparable, making the topograph relatively simple to interpret. The quartz wafer shown in Fig. 1 had two visible defects per cm^2 of illuminated area; that shown in Fig. 2 had five per cm^2 .

The above results are encouraging. Narrow bandpasses have now been shown to be obtainable from quartz at low photon energies, though the long tails in the energy scans do leave room for improvement. Similar topographs have since been taken of additional quartz wafers; these, along with deeper analysis of the image formation, will appear in a longer paper.

The authors thank Hiroshi Yamazaki for helpful discussions and early topographical measurements of the first quartz samples.

References

- Burkel, E. (1991). *Springer Tracts in Modern Physics*, Vol. 125. Berlin: Springer.
- Gerdau, E. & de Waard, H. (1999). Editors. *Nuclear Resonant Scattering of Synchrotron Radiation*, Part A. Bussum, The Netherlands: Baltzer Science. (*Hyperfine Interact.* **123/124**, 1–879.)
- Imai, Y., Yoda, Y., Zhang, X. W. & Kikuta, S. (2001). SPring-8 User Experiment Report No. 8 (2001B), p. 70. SPring-8, Hyogo, Japan.
- Imai, Y., Yoda, Y., Zhang, X. W. & Kikuta, S. (2002). SPring-8 User Experiment Report No. 9 (2002A), p. 74. SPring-8, Hyogo, Japan.
- Kihara, K. (1990). *Eur. J. Mineral.* **2**, 63–77.
- Lucht, M., Lerche, M., Wille, H.-C., Shvyd'ko, Yu. V., Rüter, H. D., Gerdau, E. & Becker, P. (2003). *J. Appl. Cryst.* **36**, 1075–1081.
- Shvyd'ko, Yu. V. & Gerdau, E. (1999). *Hyperfine Interact.* **123/124**, 741–776.
- Sutter, J. P., Baron, A. O. R., Ishikawa, T. & Yamazaki, H. (2005). *J. Phys. Chem. Solids*, **66**, 2306–2309.
- Tamasaku, K., Tanaka, Y., Yabashi, M., Yamazaki, H., Kawamura, N., Suzuki, M. & Ishikawa, T. (2001). *Nucl. Instrum. Methods Phys. Res. A*, **467–468**, 686–689.
- Yabashi, M., Tamasaku, K., Kikuta, S. & Ishikawa, T. (2001). *Rev. Sci. Instrum.* **72**, 4080–4083.
- Yoshimura, J. & Kohra, K. (1976). *J. Cryst. Growth*, **33**, 311–323.
- Yoshimura, J., Miyazaki, T., Wada, T., Kohra, K., Hosaka, M., Ogawa, T. & Taki, S. (1979). *J. Cryst. Growth*, **46**, 691–700.